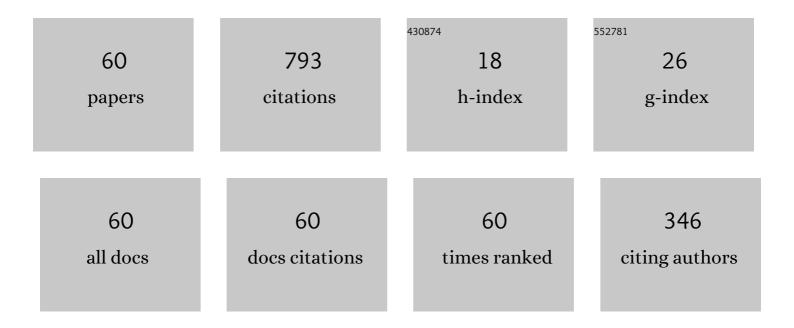
List of Publications by Year in descending order

Source: https://exaly.com/author-pdf/9214227/publications.pdf Version: 2024-02-01



DONG YANG

#	Article	IF	CITATIONS
1	Progress in octahedral spherical hohlraum study. Matter and Radiation at Extremes, 2016, 1, 8-27.	3.9	106
2	Experimental progress of inertial confinement fusion based at the ShenGuang-III laser facility in China. Nuclear Fusion, 2019, 59, 032006.	3.5	40
3	First demonstration of improving laser propagation inside the spherical hohlraums by using the cylindrical laser entrance hole. Matter and Radiation at Extremes, 2016, 1, 2-7.	3.9	39
4	First Investigation on the Radiation Field of the Spherical Hohlraum. Physical Review Letters, 2016, 117, 025002.	7.8	35
5	Determination of the Hohlraum <mml:math <br="" xmlns:mml="http://www.w3.org/1998/Math/MathML">display="inline"><mml:mi>M</mml:mi></mml:math> -band Fraction by a Shock-Wave Technique on the SGIII-Prototype Laser Facility. Physical Review Letters, 2012, 109, 145004.	7.8	33
6	Studies of laser-plasma interaction physics with low-density targets for direct-drive inertial confinement fusion on the Shenguang III prototype. Matter and Radiation at Extremes, 2021, 6, .	3.9	31
7	Experimental demonstration of low laser-plasma instabilities in gas-filled spherical hohlraums at laser injection angle designed for ignition target. Physical Review E, 2017, 95, 031202.	2.1	28
8	Recent research progress of laser plasma interactions in Shenguang laser facilities. Matter and Radiation at Extremes, 2019, 4, .	3.9	28
9	Analysis of stimulated Raman backscatter and stimulated Brillouin backscatter in experiments performed on SG-III prototype facility with a spectral analysis code. Physics of Plasmas, 2014, 21, .	1.9	27
10	Simulation study of <i>Hohlraum</i> experiments on SCIII-prototype laser facility. Physics of Plasmas, 2010, 17, .	1.9	26
11	A compact flat-response x-ray detector for the radiation flux in the range from 1.6 keV to 4.4 keV. Measurement Science and Technology, 2012, 23, 065902.	2.6	25
12	Recent diagnostic developments at the 100 kJ-level laser facility in China. Matter and Radiation at Extremes, 2020, 5, .	3.9	25
13	X-ray conversion efficiency and radiation non-uniformity in the hohlraum experiments at Shenguang-III prototype laser facility. Physics of Plasmas, 2014, 21, 112709.	1.9	24
14	Angular radiation temperature simulation for time-dependent capsule drive prediction in inertial confinement fusion. Physics of Plasmas, 2015, 22, .	1.9	23
15	The influence of laser clipped by the laser entrance hole on hohlraum radiation measurement on Shenguang-III prototype. Review of Scientific Instruments, 2014, 85, 033504.	1.3	22
16	Note: Continuing improvements on the novel flat-response x-ray detector. Review of Scientific Instruments, 2011, 82, 106106.	1.3	21
17	Direct measurement of x-ray flux for a pre-specified highly-resolved region in hohlraum. Optics Express, 2015, 23, A1072.	3.4	19
18	First experimental comparisons of laser-plasma interactions between spherical and cylindrical hohir hohiraums at SGIII laser facility. Matter and Radiation at Extremes, 2017, 2, 77-86.	3.9	18

#	Article	IF	CITATIONS
19	First Octahedral Spherical Hohlraum Energetics Experiment at the SGIII Laser Facility. Physical Review Letters, 2018, 120, 165001.	7.8	16
20	Radiation flux study of spherical hohlraums at the SGIII prototype facility. Physics of Plasmas, 2016, 23,	1.9	14
21	Development of Thomson scattering system on Shenguang-III prototype laser facility. Review of Scientific Instruments, 2015, 86, 023501.	1.3	13
22	Generation and characterization of millimeter-scale plasmas for the research of laser plasma interactions on Shenguang-III prototype. Chinese Physics B, 2010, 19, 125202.	1.4	11
23	Interaction of 0.53 î¼m laser pulse with millimeter-scale plasmas generated by gasbag target. Physics of Plasmas, 2012, 19, 062703.	1.9	10
24	The radiation temperature and <i>M</i> -band fraction inside hohlraum on the SGIII-prototype laser facility. Physics of Plasmas, 2014, 21, 022704.	1.9	10
25	Uranium hohlraum with an ultrathin uranium–nitride coating layer for low hard x-ray emission and high radiation temperature. New Journal of Physics, 2015, 17, 113004.	2.9	10
26	Investigation of the cylindrical vacuum hohlraum energy in the first implosion experiment at the SGIII laser facility. Physics of Plasmas, 2018, 25, 022703.	1.9	10
27	Progress in optical Thomson scattering diagnostics for ICF gas-filled hohlraums. Matter and Radiation at Extremes, 2019, 4, .	3.9	10
28	Comparison of the laser spot movement inside cylindrical and spherical hohlraums. Physics of Plasmas, 2017, 24, 072711.	1.9	9
29	Mitigating stimulated scattering processes in gas-filled <i>Hohlraums</i> via external magnetic fields. Physics of Plasmas, 2015, 22, .	1.9	8
30	Investigating the hohlraum radiation properties through the angular distribution of the radiation temperature. Physics of Plasmas, 2016, 23, 082708.	1.9	8
31	Implementation of ultraviolet Thomson scattering on SG-III laser facility. Review of Scientific Instruments, 2018, 89, 093505.	1.3	8
32	Multiple angle measurement and modeling of M-band x-ray fluxes from vacuum hohlraum. Physics of Plasmas, 2016, 23, 092709.	1.9	6
33	Backscatter spectra measurements of the two beams on the same cone on Shenguang-III laser facility. Review of Scientific Instruments, 2018, 89, 013501.	1.3	6
34	Enhancement of the surface emission at the fundamental frequency and the transmitted high-order harmonics by pre-structured targets. High Power Laser Science and Engineering, 2019, 7, .	4.6	6
35	Investigation on laser plasma instability of the outer ring beams on SGIII laser facility. AIP Advances, 2019, 9, .	1.3	6
36	Optimization of tungsten-doped high density carbon target in inertial confinement fusion. Nuclear Fusion, 2021, 61, 126023.	3.5	6

#	Article	IF	CITATIONS
37	Investigation of the geometrical efficiency for the two-dimensional space-resolving flux detector in inertial confinement fusion. Journal of Instrumentation, 2017, 12, P08021-P08021.	1.2	5
38	First exploration of radiation temperatures of the laser spot, re-emitting wall and entire hohlraum drive source. Scientific Reports, 2019, 9, 5050.	3.3	5
39	Experimental and simulation studies on gold bubble movement in gas-filled hohlraums. Nuclear Fusion, 2019, 59, 016002.	3.5	5
40	Experimental Study of the X-Ray Radiation Source at Approximately Constant Radiation Temperature. Plasma Science and Technology, 2013, 15, 1108-1111.	1.5	4
41	Accurate and efficient characterization of streak camera using etalon and fitting method with constraints. Review of Scientific Instruments, 2011, 82, 113501.	1.3	3
42	Coupling between a laser and a prestructured target with an arbitrary structure period. Physical Review E, 2018, 98, .	2.1	3
43	Application of the space-resolving flux detector for radiation measurements from an octahedral-aperture spherical hohlraum. Review of Scientific Instruments, 2018, 89, 063502.	1.3	3
44	Multi-keV x-ray radiator from titanium cylindrical cavity at the Shenguang-III prototype laser facility. Physics of Plasmas, 2021, 28, .	1.9	3
45	The neutron imaging system for inertial confinement fusion at the 100 kilo-Joule laser facility. Journal of Instrumentation, 2022, 17, C03026.	1.2	3
46	First Indirect Drive Experiment Using a Six-Cylinder-Port Hohlraum. Physical Review Letters, 2022, 128, .	7.8	3
47	Methods of Generation and Detailed Characterization of Millimeter-Scale Plasmas Using a Gasbag Target. Chinese Physics Letters, 2011, 28, 125202.	3.3	2
48	A Full Aperture Backscattering Light Diagnostic System Installed on the Shenguang-III Prototype Laser Facility. Plasma Science and Technology, 2014, 16, 567-570.	1.5	2
49	Demonstration of a Shock-Timing Experiment in a CH Layer at the ShenGuang III Laser Facility. Chinese Physics Letters, 2018, 35, 055202.	3.3	2
50	Stimulated Raman scattering instability of a left-handed circularly polarized laser in strongly axially magnetized plasmas. Physics of Plasmas, 2019, 26, .	1.9	2
51	Chunk mixing implosion experiments using deuterated foam capsules with gold dopant. Physical Review E, 2020, 102, 023204.	2.1	2
52	Measurement of Time-Dependent Drive Flux on the Capsule for Indirectly Driven Inertial Confinement Fusion Experiments. Physical Review Letters, 2022, 128, 075001.	7.8	2
53	Frequency mismatch in stimulated scattering processes: An important factor for the transverse distribution of scattered light. Physics of Plasmas, 2016, 23, 063303.	1.9	1
54	Potential terahertz radiation by mode conversion from two-color laser to surface plasma waves. AIP Advances, 2017, 7, .	1.3	1

#	Article	IF	CITATIONS
55	Controlling of the electromagnetic solitary waves generation in the wake of a two-color laser. Physics of Plasmas, 2018, 25, .	1.9	1
56	X-ray fluorescence imaging of jet flow in laser driven high-energy-density experiments. Physics of Plasmas, 2019, 26, 072702.	1.9	1
57	Measurement of P2 M-band flux asymmetry in indirect-drive hohlraum on Shenguang-III prototype laser facility. Review of Scientific Instruments, 2019, 90, 043505.	1.3	1
58	Optimization of x-ray emissions with Gd + Au + Gd sandwich design. AIP Advances, 2021, 11, 025005.	1.3	1
59	Implementation of a large-aperture Thomson scattering system for diagnosing driven ion acoustic waves on Shenguang-III prototype laser facility. Journal of Instrumentation, 2022, 17, P05017.	1.2	1
60	Investigation of preheat induced degradation on material compression for double shock drive under different picket power. Plasma Physics and Controlled Fusion, 2020, 62, 105015.	2.1	0